

Article

# Formation of Cellular Structure on Metastable Solidification of Undercooled Eutectic CoSi-62 at. %

Sangho Jeon and Douglas M. Matson \*

Department of Mechanical Engineering, Tufts University, Medford, MA 02155, USA; sangho.jeon@tufts.edu

\* Correspondence: douglas.matson@tufts.edu; Tel.: +1-617-627-3239

Academic Editor: Geun Woo Lee

Received: 13 August 2017; Accepted: 27 September 2017; Published: 30 September 2017

**Abstract:** The relationship between emissivity, delay time, and surface growth for metastable solidification of CoSi-62 at. % eutectic alloys is reported from undercooling experiments conducted using electrostatic levitation. A fraction of the undercooled melt is first solidified to CoSi<sub>2</sub> with subsequent nucleation in the mushy-zone of CoSi after an observed delay time. During this double recalescence event, the temperature of the secondary recalescence exceeds the liquidus, indicating that the spectral emissivity has changed. This emissivity change increases with longer delay times during solidification and is linked to the growth of cellular structure on the sample surface. Density measurements showed that the cellular structure begins to grow rapidly at a certain time during metastable solidification. This phenomenon is likely associated with the constitutional undercooling of the remaining melt.

**Keywords:** CoSi-CoSi<sub>2</sub> eutectic; undercooling; metastable solidification; emissivity; electrostatic levitation; cellular structure

## 1. Introduction

Crystallization is one of the fundamental issues in materials science and condensed matter physics due to its critical role in understanding the processes of nucleation, solidification, and solid-state phase transformation. It is also of significant importance in alloy design and in the control of single crystal growth. Various crystallization pathways and growth mechanisms of deeply supercooled [1–4], supersaturated [5,6], and even super-compressed [7–9] metastable phases were extensively reported based on various experimental techniques using electrostatic levitation (ESL), electromagnetic levitation (EML), aerodynamic levitation (ADL), and diamond anvil cell (DAC).

In metallic liquids, crystallization pathways and growth morphology evolution depend on the degree of undercooling. If the undercooling exceeds a critical amount, some alloy classes show double recalescence, where solidification proceeds through a metastable phase before a thermodynamically stable phase forms. Here, there is a two-phase region where the metastable solid and the remaining liquid coexist in a condition known as the mushy-zone. Solute partitioning and rejection cause gradients of temperature and composition with subsequent deviation from the equilibrium phase diagram; the remaining liquid may be significantly constitutionally undercooled in the mushy-zone. Then, competitive nucleation and growth of the metastable and stable phases determine the growth kinetics [10–13] and evolution of the final microstructure [14–16]. The microstructure depends on the ratio of temperature gradient and crystal growth rate [17] combined with interfacial kinetics [18,19]. These are also influenced by fluid flow (or convection), because fluid flow affects the heat and mass transport at the solid-liquid interface [14]. However, direct observation of surface growth during the metastable solidification of alloys consisting of two-line compounds has not been reported in experiments. In the present work, a CoSi-CoSi<sub>2</sub> eutectic alloy at composition of CoSi-62 at. % was chosen as a model system due to its unique features [14] to allow an investigation of the

relationship between delay time and surface growth on metastable solidification in the mushy-zone from undercooling experiments using electrostatic levitation (ESL). An emissivity change was observed during double recalescence of the melt. This phenomenon relates to the delay time as a function of undercooling with associated change in surface morphology. Density measurements were conducted during the cooling process to observe how these changes are related to each other and what factors affect their relevance.

## 2. Materials and Method

CoSi-62 at. % alloys (Co 99.95%, Si 99.995%/Alfa Aesar, Haverhill, MA, USA) were prepared by arc-melting the pure element under an Ar atmosphere. A zirconium sphere was used as an oxygen getter to reduce the remaining oxygen in the arc-melting chamber prior to the melting of the elements. The amount of mass evaporation during the arc-melting was less than 0.2% of the initial mass. The ESL facility at the NASA Marshall Space Flight Center (MSFC) in Huntsville, AL was used to study the crystallization behavior of melts. Samples with a mass of approximately 35 mg (a diameter of ~2 mm) were levitated between two electrodes and melted by using a high voltage amplifier and a Nd:YAG high-power laser under an ultra-high vacuum (UHV) condition of  $\sim 10^{-7}$  Torr. The temperature of the sample was monitored with a Mikron MI-GA140 single-color pyrometer with a spot size of ~0.8 mm, which was operated at a wavelength range of 1.45  $\mu\text{m}$ –1.8  $\mu\text{m}$ . After several thermal cycles in the ESL, the amount of mass evaporation was held to less than 1.5% of the initial mass. For density evaluation, a UV back-light was used to capture a shadow of levitated samples into a high-speed camera. The camera was focused such that radial color gradient across the edge of the projected sample image was between 4 and 8 pixels. A tungsten-carbide sphere with a diameter of 2.2 mm was used for the calibration to establish the required pixel-to-meter conversion factor. During the density analysis procedure, the midpoint of the color gradient across the edge of the sample was found and the encompassed area was taken to be the projected area of the sample [20]. After the ESL experiments, the microstructure of the samples was observed using a Phenom ProX scanning electron microscopy (SEM) in back-scatter mode.

## 3. Results and Discussion

### 3.1. Time-Temperature Profiles and Delay Time

Figure 1a shows the representative time-temperature profile of a CoSi-62 at. % alloy during heating and cooling in the ESL. The solid alloy is heated up to its liquidus temperature ( $T_l$ ) near 1587 K, and the liquid is heated up to a desired temperature to dissolve the oxygen-containing phases of the melt [21]. This overheating allows the melt to be undercooled deeply below its  $T_l$  when the heating laser is turned off. After undercooling, the melt often shows double recalescence on solidification where a fraction of the melt is first solidified as a primary phase, with subsequent solidification to a second phase after a delay time given by the duration of the intervening thermal plateau. Previous studies showed that the primary and secondary phases are  $\text{CoSi}_2$  and  $\text{CoSi}$ , respectively, based on an in situ synchrotron X-ray diffraction experiment [15] and microstructure evaluations [14,15] when samples are undercooled deeply. This phase sequence is also supported by comparing the interfacial free energy and nucleation barrier of the two phases based on the classical nucleation theory [14,15]. A small hump before the secondary recalescence is often observed, but its origin is still unclear.

Figure 1b shows changes of delay time as a function of undercooling of the melt, which indicates three distinct regions of behavior. At low undercoolings, the delay time linearly decreases with undercooling, and it reaches close to zero in an intermediate undercooling region. The delay time rises rapidly at critical undercooling and decreases again at high undercoolings. However, its initial value is much longer than observed at low undercoolings. In general, the delay time is determined by the combination of an incubation time for nucleation of the secondary phases and a thermal balance between the remaining melt and the freezing primary phase. Therefore, the change of

the delay time behavior between low and high undercoolings means that the primary phase was changed; thus, phase selection depends on the degree of undercooling. Li et al. [15] suggested that at low undercoolings, CoSi solidifies primarily as the leading phase with a single recalescence event (zero delay time). On the other hand, Zhang et al. [14] showed that a two-step recalescence is found in both low and high undercoolings, and the primary phase is CoSi at low undercoolings. Therefore, it is supposed that the sequence of primary phase formation is reversed at low undercoolings, but it seems to be more complicated at an intermediate undercooling with the nearly zero-delay behavior. The remainder of the paper will deal with analysis of the high undercooling region with primary CoSi<sub>2</sub> and secondary CoSi solidification, and details of the phase sequence will be discussed in future work.

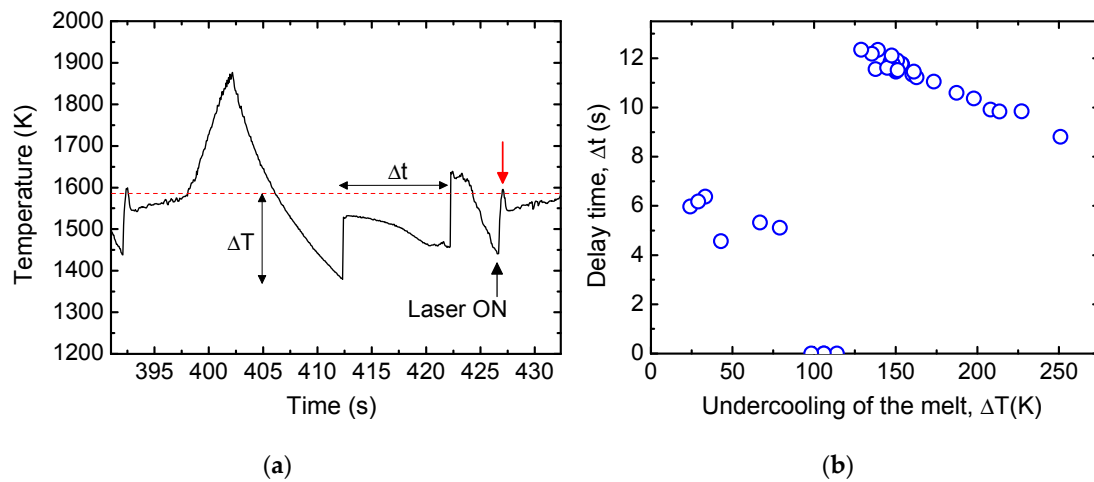


**Figure 1.** (a) Representative time-temperature profile of a CoSi-62 at. % alloy processed in the electrostatic levitator (ESL). The liquidus temperature (marked by a red dotted line) was determined based on the Co-Si phase diagram. (b) Changes of delay time as a function of undercooling of the melt. The delay time shows three distinct regions of behavior.

### 3.2. Emissivity Change during Solidification

As shown in Figure 1a, the recalescence temperature for the secondary CoSi phase exceeds the liquidus (marked by a red dotted line in Figure 1a) of the bulk composition, and is associated with a sudden temperature drop of about 80 K (marked by a red arrow in Figure 1a) on a subsequent heating cycle. This drop of temperature signal is likely attributed to the changing spectral emissivity with temperatures. In general, the emissivity for solids is strongly dependent on surface roughness and surface layers of oxides, making it a more extrinsic property. In contrast, liquid surfaces are smoother and therefore should provide more intrinsic values [22,23]. In the mushy-zone, therefore, these two effects have to be considered together. Figure 2a shows the comparison of the time-temperature profiles of samples having different undercoolings of the melt. It is found that the recalescence temperature ( $T_{R1}$ ) of primary CoSi<sub>2</sub> phases does not depend on undercooling (Figure 2b). However, the remaining melt becomes more Co-rich than the bulk composition as the undercooling increases. After recalescence, the fraction solid of a CoSi-62 at. % phase can be predicted by the Stefan Equation:

$$C_p \Delta T = f_s \Delta H_f \quad (1)$$

where  $C_p$  is the specific heat,  $\Delta T$  is the undercooling, and  $f_s$  and  $\Delta H_f$  are the fraction solid and heat of fusion, respectively. Using the data of  $C_p$  and  $\Delta H_f$  at the melting temperature (42 J/mol·K [24] and 35678 J/mol [25]), one can estimate the  $f_s$  to be 0.179 and 0.302 for undercoolings of 152 K and 257 K, respectively. Furthermore, one can estimate compositions of the remaining melt to be CoSi-60.9 at. % and CoSi-60 at. %, respectively. This small difference in the composition is due to a similar stoichiometric composition between CoSi<sub>2</sub> and the bulk melt. Additionally, the independent

measurement of  $\text{CoSi}_2$  alloys shows little emissivity change upon nucleation of their melt with different degree of undercoolings (not shown). Therefore, it is concluded that the emissivity difference of the solid and liquid phases is negligible in the measured undercooling regions, and thus the primary recalescence temperature is nearly independent of undercooling.

Unlike the primary recalescence temperature, that of secondary  $\text{CoSi}$  phases decreases with higher undercoolings, as shown in Figure 2c. Moreover, it is found that the degree of the temperature drop on the heating process is proportional to the delay time (thus undercooling), as shown in Figure 3. This relation means that the emissivity change occurs during the delay period prior to secondary recalescence and thus is likely associated with the accumulation of surface roughness.

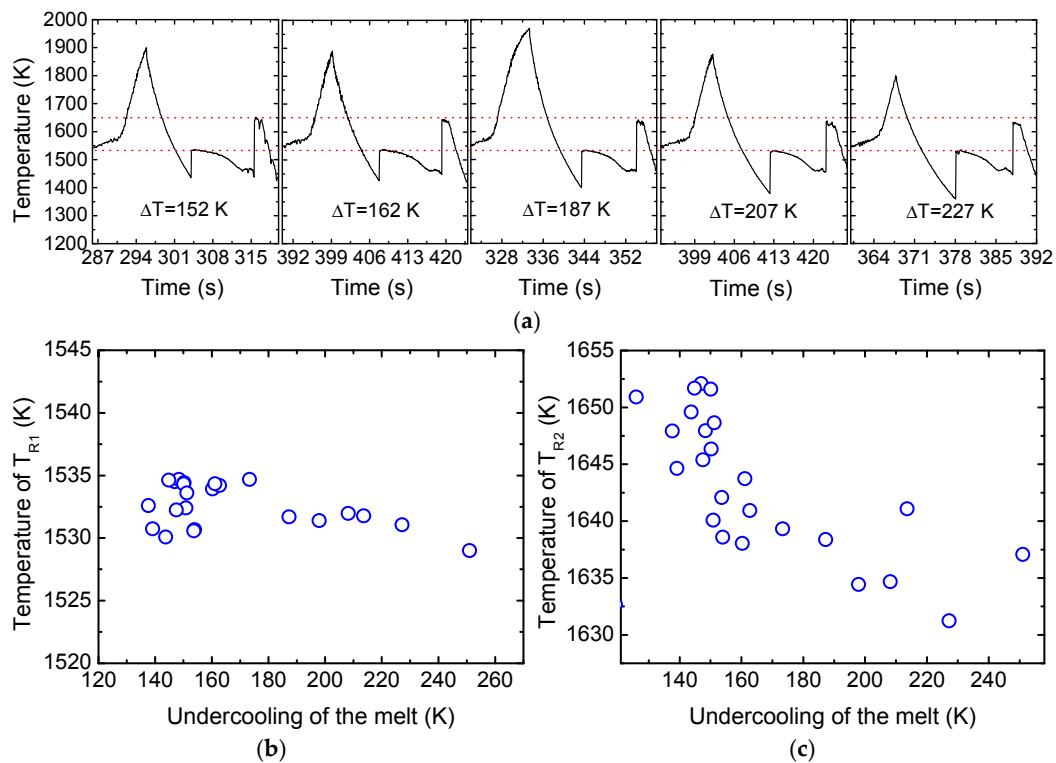


**Figure 2.** (a) Illustration of time-temperature profiles for different undercoolings. Changes of the recalescence temperature for (b) primary ( $\text{CoSi}_2$ ) and (c) secondary ( $\text{CoSi}$ ) phases as a function of undercooling of the melt.

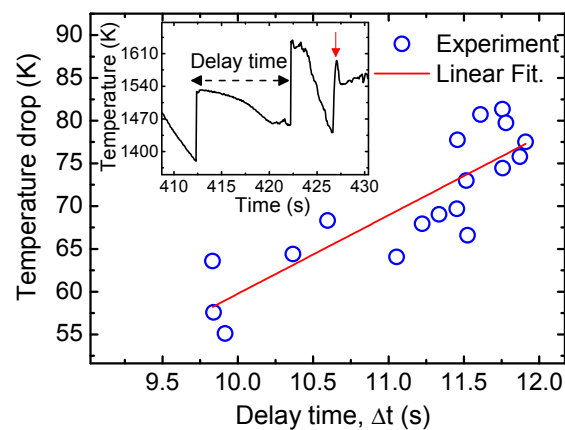


**Figure 3.** Relation between temperature drop (marked by a red arrow in inset) on heating curve and delay time. The degree of the temperature drop increases with increasing delay time.

### 3.3. Microstructure and Density Measurements

Figure 4 shows back-scattered SEM micrographs of the surface of four samples that were radiatively cooled during ESL testing. Those samples attain low (43 K), medium (98 K), and high (145 K and 252 K) undercoolings prior to solidification, respectively.

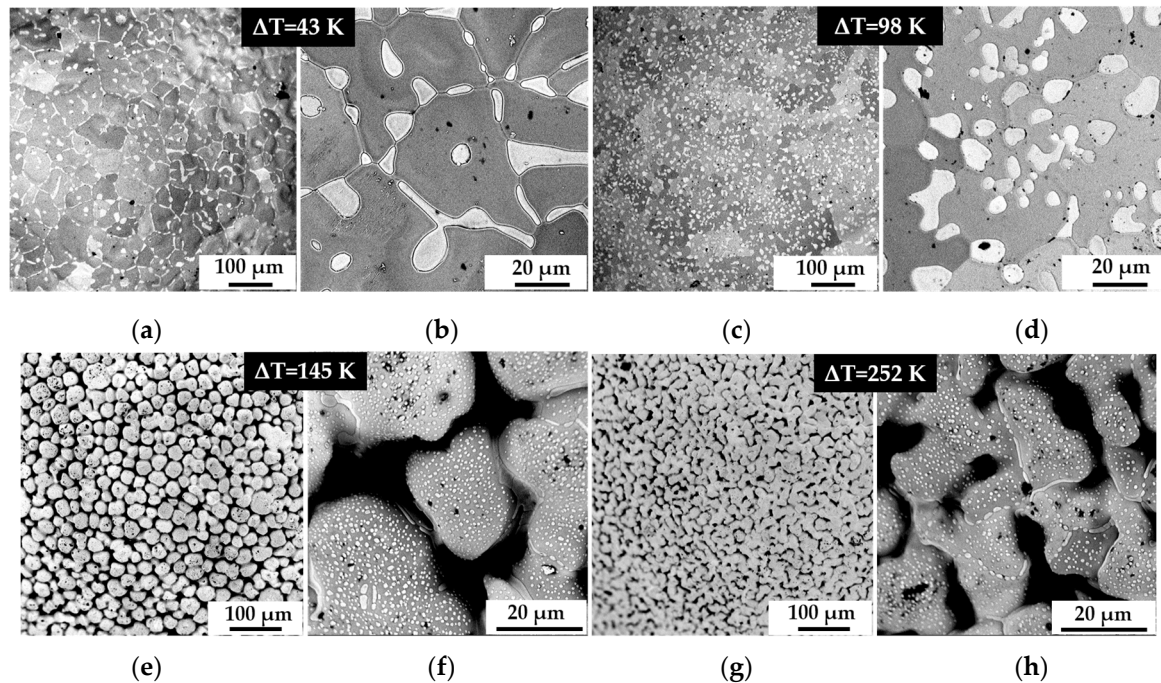


**Figure 4.** Back-scattered SEM micrographs for the surface of CoSi-62 at. % alloys processed (radiatively cooled) in the ESL. (a,b) Low ( $\Delta T = 43$  K,  $\Delta t = 4.57$  s), (c,d) medium ( $\Delta T = 98$  K,  $\Delta t = \sim 0$  s), (e,f) high ( $\Delta T = 145$  K,  $\Delta t = 12.13$  s), and (g,h) high ( $\Delta T = 252$  K,  $\Delta t = 8.88$  s) undercoolings.

At the low undercooling, the surface shows CoSi particles (white contrast) and CoSi<sub>2</sub> grains (dark contrast). The coarsened CoSi particles are identified as the primary phase, since each of them is enveloped by the growth of the CoSi<sub>2</sub> grains. At the medium undercooling, the grain size of CoSi<sub>2</sub> phases is increased, and rounded-like CoSi particles are observed.

However, the surface shows a dramatic change in structure at the high undercoolings, which shows a cellular-like structure due to the significant coarsening of the proto-dendritic structure formed during recalescence. This is clearly seen for the sample with an undercooling of 145 K, which experienced significant coarsening during the long delay time. Small dots of white contrast in Figure 4f,h were confirmed as CoSi, which are formed during secondary recalescence. Therefore, it is supposed that the emissivity change is associated with the surface roughness of the cellular-like structure rather than the nucleation of CoSi. The cellular structure exhibits a non-planar view factor with more surface which can emit more radiative energy. Thus, it has high emissivity. This microstructural evidence also supports the previous observation (Figure 1b) that three growth regimes occur as a function of delay time.

The density measurements provided more evidence for the change of the surface roughness. Figure 5a shows the time-density (right axis) and time-temperature (left axis) profiles of a sample with  $\Delta T = 207$  K during solidification. Unlike in cases of other metallic melts, the density shows an unusual aspect with distinct regions of behavior. First, a fraction of the melt is solidified to the metastable CoSi<sub>2</sub> phase, and grows across the entire surface of the droplet (see region A in Figure 5a), and therefore the density increases. However, the density begins to slightly decrease (see region B in Figure 5a) from a certain time before the second recalescence. The density of crystalline materials usually decreases

in solidification. Therefore, this decrease should be viewed as a change of apparent density and can be understood as follows. Following the primary growth of  $\text{CoSi}_2$  in metastable solidification at high undercoolings, the remaining melt becomes more Co-rich liquid than the bulk composition, and its liquidus temperature increases based on the equilibrium Co-Si phase diagram. In this case, the melt becomes constitutionally undercooled, because the cellular structure can grow under such conditions. Figure 5b shows surface images of the droplet during the solidification of the melt. The sample surface at time interval A (marked by the first red arrow in Figure 5a) shows a smooth surface, while at time interval B the surface is characterized by significant roughness (marked by the second red arrow in Figure 5a). This change of the surface roughness can be ascribed to liquid decanting from the sample surface driven by Marangoni convection, and viewed as the sign of the occurrence of a constitutional undercooling of the remaining melt during time interval B.

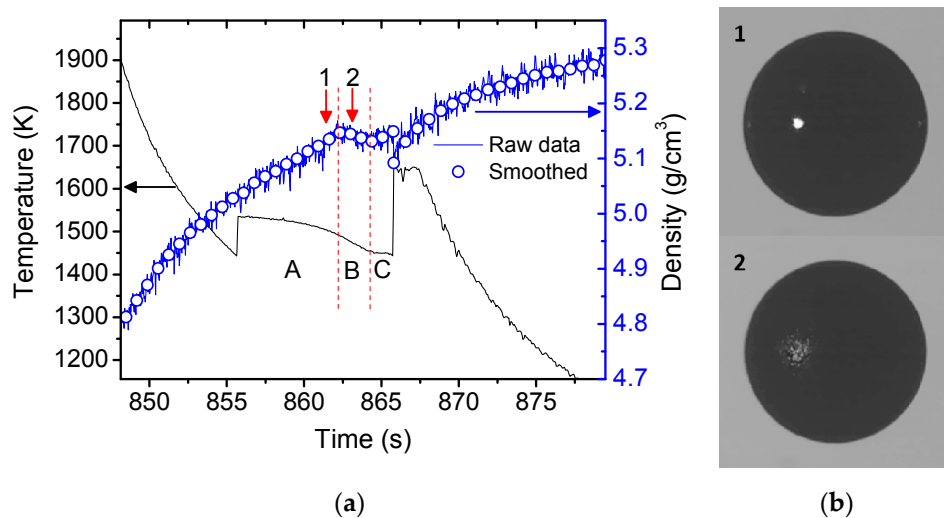


**Figure 5.** (a) Time-density and time-temperature profiles of a CoSi-62 at. % melt during solidification. The density shows a distinct behavior dependence on delay time. (b) Video images captured at A and B regions. The corresponding times to the images are 861.4 s and 863.1 s for points 1 and 2, respectively.

Since density generally is evaluated based on the edge detection of levitated liquid or solid droplets in a levitation experiment [26,27], the volume in time interval B of Figure 5a can be overestimated due to the cellular structure, resulting in a decrease in the observed apparent density. As shown in Figure 5b, the sudden change of surface roughness due to liquid decanting from the sample surface strongly supports this behavior. After the formation of the cellular structure, the density increases again (see region C in Figure 5a). The following sudden drop of the density upon the secondary recalescence is due to partial melting of the  $\text{CoSi}_2$  phase, and is consistent with the lowering of the thermal plateau temperature.

Figure 6a shows the time-temperature curve of a sample that has a short delay time of about 5.5 s. Unlike the profile shown in Figure 1a, the secondary recalescence temperature does not exceed the liquidus one of the bulk alloy, and no temperature drop is observed upon subsequent heating. This contrast in the thermal behavior also demonstrates that the emissivity change is associated with the constitutional undercooling of the remaining melt following metastable solidification with the primary growth of  $\text{CoSi}_2$ . Initially, the spectral emissivity of the liquid is assumed to be 0.25, but during this isothermal temperature hold the temperature appears to change, and this change can be re-evaluated based on the calculation of the emissivity shift. The data are plotted as a function of delay time in Figure 6b. If the experimental data are extrapolated to a critical delay time of 4.3 s, one may find that there is no emissivity change (or apparent temperature drop). This result is in agreement with the experimental observation of Figure 6a.

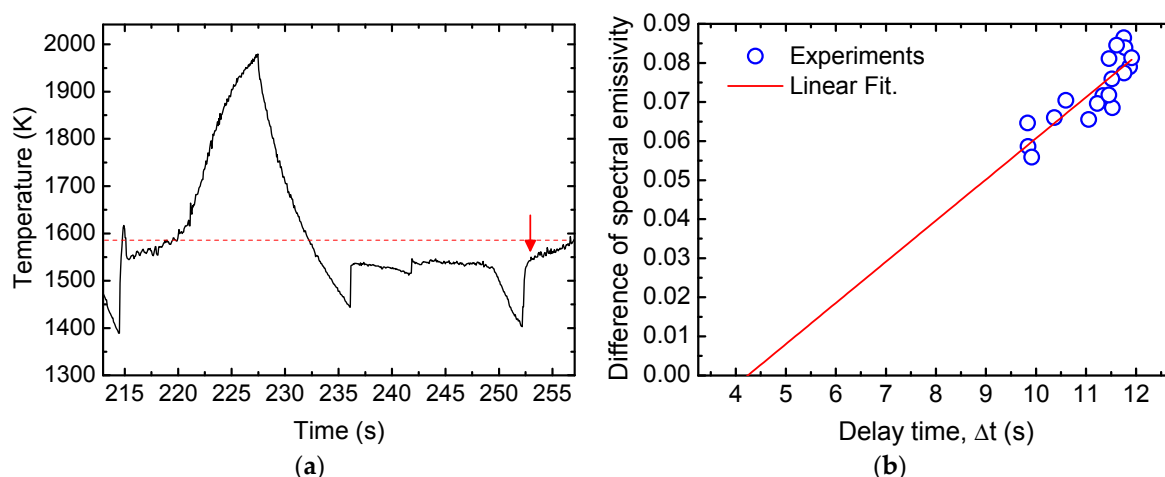


**Figure 6.** (a) Time-temperature profile of a CoSi-62 at. % alloy with a short delay time. No temperature drop (marked by a red arrow) is observed on the subsequent heating curve. (b) Relation between delay time and change of spectral emissivity. The emissivity change for the temperature drop was calculated by assuming the emissivity of the liquid phase to be 0.25.

#### 4. Conclusions

In summary, the metastable solidification of CoSi-62 at. % eutectic alloys in an ESL facility has been investigated. At high undercoolings, double recalescence events have been observed where the CoSi<sub>2</sub> phase is first nucleated and the CoSi phase follows after a delay time in the mushy-zone. A change of spectral emissivity has been observed during the second event. This change increases with the delay time and has been correlated with the formation of a cellular structure. It has been shown that the cellular structure evolves shortly before the second recalescence and is most likely a result of the constitutional undercooling of the remaining melt. This work represents the first direct observation of the growth of cellular structures during metastable solidification in the mushy-zone that influences surface emissivity.

**Acknowledgments:** We would like to thank Jianrong Gao for useful discussions, Glenn Fountain and Trudy L. Allen for technical assistance at NASA Marshall Space Flight Center (MSFC), and Gabrielle M. String for technical assistance on SEM measurement. The work at Tufts University was partially funded by NASA, under the ELFSTONE grant NNX16AB59G.

**Author Contributions:** D.M.M. conceived and designed the experiments; D.M.M. performed the experiments; S.J. and D.M.M. analyzed the data; S.J. and D.M.M. contributed reagents/materials/analysis tools; S.J. and D.M.M. wrote the paper.

**Conflicts of Interest:** The authors declare no conflict of interest.

#### References

1. Sung, Y.S.; Takeya, H.; Hirata, K.; Togano, K. Spherical Nb single crystals containerless grown by electrostatic levitation. *Appl. Phys. Lett.* **2003**, *82*, 3638–3640.
2. Russo, J.; Romano, F.; Tanaka, H. New metastable form of ice and its role in the homogeneous crystallization of water. *Nat. Mater.* **2014**, *13*, 733–738. [[PubMed](#)]
3. Herlach, D.M. Dendrite growth kinetics in undercooled melts of intermetallic compounds. *Crystals* **2015**, *5*, 355–375. [[CrossRef](#)]
4. Herlach, D.M.; Palberg, T.; Klassen, I.; Klein, S.; Kobold, R. Overview: Experimental studies of crystal nucleation: Metals and colloids. *J. Chem. Phys.* **2016**, *145*, 211703. [[PubMed](#)]

5. Lee, S.; Wi, H.S.; Jo, W.; Cho, Y.C.; Lee, H.H.; Jeong, S.-Y.; Kim, Y.-I.; Lee, G.W. Multiple pathways of crystal nucleation in an extremely supersaturated aqueous potassium dihydrogen phosphate (KDP) solution droplet. *Proc. Natl. Acad. Sci. USA* **2016**, *113*, 13618–13623. [[CrossRef](#)] [[PubMed](#)]
6. Lee, S.; Jo, W.; Cho, Y.C.; Lee, H.H.; Lee, G.W. Solution electrostatic levitator for measuring surface properties and bulk structures of an extremely supersaturated solution drop above metastable zone width limit. *Rci. Sci. Instrum.* **2017**, *88*, 055101. [[CrossRef](#)] [[PubMed](#)]
7. Tateno, S.; Hirose, K.; Ohishi, Y.; Tatsumi, T. The structure of iron in earth's inner core. *Science* **2010**, *330*, 359–361. [[CrossRef](#)] [[PubMed](#)]
8. Lin, C.; Smith, J.S.; Sinogeikin, S.V.; Kono, Y.; Park, C.; Kenney-Benson, C.; Shen, G. A metastable liquid melted from a crystalline solid under decompression. *Nat. Commun.* **2017**, *8*, 14260. [[PubMed](#)]
9. Lee, G.W.; Evans, W.J.; Yoo, C.-S. Crystallization of water in a dynamic diamond-anvil cell: Evidence for ice VII-like local order un supercompressed water. *Phys. Rev. B* **2006**, *74*, 134112.
10. Rodriguez, J.E.; Kreischer, C.; Volkmann, T.; Matson, D.M. Solidification velocity of undercooled Fe-Co alloys. *Acta Mater.* **2017**, *122*, 431–437. [[CrossRef](#)]
11. Wu, Y.H.; Chang, J.; Wang, W.L.; Wei, B. Metastable couple-growth kinetics between primary and peritectic phases of undercooled hypoperitectic Fe<sub>54.5</sub>Ti<sub>45.5</sub> alloy. *Appl. Phys. Lett.* **2016**, *109*, 154101. [[CrossRef](#)]
12. Hermann, R.; Loser, W. Growth kinetics of undercooled Fe-Co melts. *J. Magn. Magn. Mater.* **2002**, *242–245*, 285–287. [[CrossRef](#)]
13. Matson, D.M. Growth competition during double recalescence in Fe-Cr-Ni alloys. *MRS Online Proceedings Library Archive* **1998**, *551*, 227–234. [[CrossRef](#)]
14. Zhang, Y.K.; Gao, J.; Kolbe, M.; Klein, S.; Yang, C.; Yasuda, H.; Herlach, D.M.; Gandin, C.-A. Phase selection and microstructure formation in undercooled Co-61.8 at. % melts under various containerless processing conditions. *Acta Mater.* **2013**, *61*, 4861–4873. [[CrossRef](#)]
15. Li, M.; Nagashio, K.; Ishikawa, T.; Mizuno, A.; Adachi, M.; Watanabe, M.; Yoda, S.; Kuribayashi, K.; Katayama, Y. Microstructure formation and in situ phase identification from undercooled Co-61.8 at.% Si melts solidified on an electromagnetic levitator and an electrostatic levitator. *Acta Mater.* **2008**, *56*, 2514–2525. [[CrossRef](#)]
16. Prashanth, K.G.; Eckert, J. Formation of metastable cellular microstructures in selective laser melted alloys. *J. Alloys Compd.* **2017**, *707*, 27–34. [[CrossRef](#)]
17. Tiller, W.A.; Jackson, K.A.; Rutter, J.W.; Chalmers, B. The redistribution of solute atoms during the solidification of metals. *Acta Metall.* **1953**, *1*, 428–437. [[CrossRef](#)]
18. Sekerka, R.F. Application of the time-dependent theory of interface stability to an isothermal phase transformation. *J. Phys. Chem. Solids* **1967**, *28*, 983–994. [[CrossRef](#)]
19. McKeown, J.T.; Kulovits, A.K.; Liu, C.; Zweiaccker, K.; Reed, B.W.; LaGrange, T.; Wiezorek, J.M.K.; Campbell, G.H. In situ transmission electron microscopy of crystal growth-mode transitions during rapid solidification of a hypoeutectic Al-Cu alloy. *Acta Mater.* **2014**, *65*, 56–69. [[CrossRef](#)]
20. Lee, J.; Rodriguez, J.E.; Hyers, R.W.; Matson, D.M. Measurement of density of Fe-Co alloys using electrostatic levitation. *Metall. Trans. B* **2015**, *46B*, 247–2475. [[CrossRef](#)]
21. Mukherjee, S.; Zhou, Z.; Johnson, W.L.; Rhim, W.K. Overheating threshold and its effect on time-temperature-transformation diagrams of zirconium based bulk metallic glasses. *Appl. Phys. Lett.* **2004**, *84*, 5010–5012. [[CrossRef](#)]
22. Gangopadhyay, A.K.; Kelton, K.F. Measurement of the temperature-dependent total hemispherical emissivity using and electrostatic levitation facility. *Int. J. Thermophys.* **2017**, *39*, 1–8. [[CrossRef](#)]
23. Kawamura, H.; Fukuyama, H.; Watanabe, M.; Hibiya, T. Normal spectral emissivity of undercooled liquid silicon. *Meas. Sci. Technol.* **2005**, *16*, 386–393. [[CrossRef](#)]
24. Barth, M.; Wei, B.; Herlach, D.M. Crystal growth in undercooled melts of the intermetallic compounds FeSi and CoSi. *Phys. Rev. B* **1995**, *51*, 3422–3428. [[CrossRef](#)]
25. Zhang, L.; Du, Y.; Xu, H.; Pan, Z. Experimental investigation and thermodynamic description of the Co-Si system. *Calphad* **2006**, *30*, 470–481. [[CrossRef](#)]

26. Bradshaw, R.C.; Schmidt, D.P.; Rogers, J.R.; Hyers, R.W. Machine vision for high-precision volume measurement applied to levitated containerless material processing. *Rev. Sci. Instrum.* **2005**, *76*, 125108. [[CrossRef](#)]
27. Yoo, H.; Park, C.; Jeon, S.; Lee, S.; Lee, G.W. Uncertainty evaluation for density measurements of molten Ni, Zr, Nb and Hf by using a containerless method. *Metrologia* **2005**, *52*, 677–684. [[CrossRef](#)]



© 2017 by the authors. Licensee MDPI, Basel, Switzerland. This article is an open access article distributed under the terms and conditions of the Creative Commons Attribution (CC BY) license (<http://creativecommons.org/licenses/by/4.0/>).